

Potential field-based approaches for nanobotics in drug delivery

Leonardo Kamajaya¹, Indrazno Siradjuddin¹, Gillang Al Azhar¹, Fitri¹, Agwin Fahmi Fahanani²

¹Department of Electronics Engineering, Faculty of Electrical Engineering, State Polytechnic of Malang, Malang, Indonesia

²Department of Physiology, Faculty of Medicine, Universitas Brawijaya, Malang, Indonesia

Article Info

Article history:

Received Mar 4, 2025

Revised Oct 17, 2025

Accepted Nov 23, 2025

Keywords:

Drug delivery

Local minima

Nanorobotics

Obstacle avoidance

Potential field

ABSTRACT

Nanorobotics has transformed targeted drug delivery by enhancing therapeutic efficacy, minimizing off-target effects, and increasing precision. However, navigating complex biological environments is challenging. In the field of macroscopic robotics, potential field (PF)-based approaches that utilize attractive and repulsive virtual forces provide a promising framework that can be applied to path planning for nanorobots. This study modifies PF algorithms for nanorobotic navigation to address challenges such as avoiding dynamic obstacles, escaping local minima, and optimizing trajectories in real time. We evaluated the movement of the nanorobot through simulations under static and dynamic conditions for the targets and obstacles. The results demonstrate that nanorobotics with hybrid PF methodologies enhance navigation performance, enabling nanorobots to successfully navigate through biological barriers and efficiently reach their target locations. This work is a significant step towards intelligent and autonomous nanorobotic drug delivery systems and contributes to practical biomedical applications.

This is an open access article under the [CC BY-SA](#) license.



Corresponding Author:

Agwin Fahmi Fahanani

Department of Physiology, Faculty of Medicine, Universitas Brawijaya, Malang, Indonesia

Jl. Veteran No. 10-11, Malang, East Java, Indonesia

Email: agwinfahmi@ub.ac.id

1. INTRODUCTION

Nanorobotics has revolutionized targeted drug delivery by offering greater accuracy in complex biological environments. Conventional methods suffer from systemic toxicity, limited precision, and inefficient traversal of physiological barriers. In contrast, nanorobots offer precise treatment delivery, minimize unintended effects, and enhance therapeutic outcomes [1]-[3]. Despite these technological developments, effectively navigating complex and dynamic biological environments remains challenging.

The application of potential field (PF) techniques, which have been widely utilized in path planning for large-scale robotics, presents a promising framework for guiding nanorobots [4], [5]. These algorithms simulate attractive and repulsive forces to facilitate real-time trajectory adjustment. However, conventional PF techniques are susceptible to limitations, such as local minima and insufficient adaptability to dynamic targets [6]. Despite recent advancements in hybrid PF approaches that address specific limitations, further enhancements are necessary to ensure their effective implementation at the nanoscale.

Unlike traditional PF methods tailored for macroscopic robots [4], [6], [7], this study presents a nanoscale-adapted PF framework that incorporates adaptive kinematics, real-time trajectory adjustments, and hybrid control mechanisms for navigating biological microenvironments. Building on recent advancements

in artificial potential field (APF) models, such as the bacterial PF approach [5], the proposed method extends these principles to nanoscale drug delivery. It does so by integrating dynamic force field modeling capable of managing both static and dynamic obstacles with minimal path deviation. This nanoscale adaptation addresses challenges related to viscous drag, Brownian motion, and environmental uncertainties, thereby improving trajectory convergence, stability, and responsiveness. Overall, the approach significantly advances the practical implementation of autonomous nanorobotic navigation for precise and efficient targeted drug delivery.

2. THEORETICAL APPROACH

2.1. Potential field

PF algorithms create virtual force fields to direct robots towards targets (attractive forces, F_a) and away from obstacles (repulsive forces, F_r) [8]-[10]. The cumulative force (F_x) applied on a robot is articulated as:

$$F_x = F_a + F_r \quad (2.1)$$

In a fundamental PF scenario, the robot perceives barriers as repulsive PFs and the objective as an appealing field. Let $\mathbf{x} = (x, y)^T$ signify the robot's position, thereafter the area in which the robot operates is referred to as: $U(\mathbf{x})$, where:

$$U(\mathbf{x}) = U_a(\mathbf{x}) + U_r(\mathbf{x}) \quad (2.2)$$

and $U_a(\mathbf{x})$ denotes the attractive field and $U_r(\mathbf{x})$ expresses the repulsive field. It may also be expressed as:

$$U(\mathbf{x}) = U_a(\mathbf{x}) + \sum_{n=1}^N U_r^{(n)}(\mathbf{x}) \quad (2.3)$$

where N represents the total quantity of barriers within the nanorobot's operational environment. The force propelling the nanorobot is the negative gradient of the PF, that is:

$$F_x = \underbrace{-\nabla_x U_a(\mathbf{x})}_{F_a(x)} - \underbrace{\nabla_x U_r(\mathbf{x})}_{F_r(x)} \quad (2.4)$$

where $F_a(x) = (F_{a,x}, F_{a,y})^T$ is the attractive force vector and $F_r(x) = (F_{r,x}, F_{r,y})^T$ is the repulsive force vector.

Conventional PF methods encounter challenges such as local minima, target inaccessibility, and limited dynamic obstacle-avoidance. Researchers have addressed these issues by implementing speed-dependent fields, simulated annealing, and hybrid PF global planners [8], [11], [12], thereby enhancing navigation in high-density environments.

2.2. Nanorobotics-driven drug delivery systems

Nanorobotics-driven drug delivery systems represent an innovative approach for precise medication. These nanorobot devices, typically ranging from 1 to 100 nm in size, are capable of traversing the human body to deliver pharmaceuticals directly to targeted sites [13], [14]. They employ specialized targeting mechanisms, such as ligand-receptor interactions, magnetic guidance, or enzymatic processes, to concentrate on specific problem areas, thereby minimizing side effects and enhancing therapeutic efficacy [15], [16]. Compared to conventional methods, this approach offers superior control over pharmacokinetics, necessitates lower dosages, and facilitates patient adherence to treatment regimens [17], [18].

A nanorobot consists of three primary components, such as propulsion system, drug storage compartment, and navigation unit. Propulsion may be achieved through magnetic, chemical, or enzymatic means or a combination thereof, enabling the robot to navigate through viscous bodily fluids. Navigation is directed by sophisticated algorithms that assist a robot in circumventing obstacles and maintaining its trajectory. These features are essential for the precise delivery of drugs within the body.

Although there are some challenges in this area like ensuring biocompatibility, preventing immune reactions, maintaining stability inside the body, and achieving mass production, advancements are still being made [2], [19]. Innovative solutions like biodegradable coatings, lipid carriers, and enzyme surfaces have improved the integration of these robots with biological systems. Advances in 3D printing, self-assembly, and swarm coordination have made these systems increasingly viable for medical applications [20], [21].

3. PROPOSED METHOD

3.1. Kinematic of nanorobotics

Nanorobots rely on regulated kinematic motion to achieve precise drug delivery and targeting. Their movement is influenced by ambient conditions, propulsion mechanisms and real-time feedback systems. Kinematic modeling of nanorobots involves characterizing their motion parameters, energy efficiency, and adaptation within dynamic biological environments [22], [23].

The mobility of nanorobots is characterized by the interactions between velocity and force. The propulsion force $F_{magnetic}$ for magnetic-driven nanorobots is obtained from external field gradients.

$$F_{magnetic} = \nabla(m \cdot B) \quad (3..1)$$

Where m is the magnetic moment and B is the applied field.

Nanorobotic motion is influenced by various factors, including ambient conditions and fluid viscosity, which is a key factor in determining drag forces (F_{drag}).

$$F_{drag} = 6\pi\eta rv \quad (3..2)$$

where η is fluid viscosity, r is nanorobot radius, and v is velocity.

3.2. Potential field algorithm

3.2.1. Attractive potential field

The attractive PF is defined as the quadratic of the distance between the nanorobot position and the objective position d_a^2 . The attractive PF becomes more pronounced as the nanorobot's position deviates from the objective position [24], [25]. The enticing PF function can be expressed as:

$$U_a(\mathbf{x}) = \frac{1}{2}k_a d_a^2 \quad (3..3)$$

$$= \frac{1}{2}k_a \|(\mathbf{x}^* - \mathbf{x})\|^2 \quad (3..4)$$

where k_a is the attractive PF constant and \mathbf{x}^* is the goal postion. Assuming that the goal position is static then:

$$-\nabla_{\mathbf{x}} U_a(\mathbf{x}) = -\frac{\partial U_a(\mathbf{x})}{\partial \mathbf{x}} = k_a \|(\mathbf{x}^* - \mathbf{x})\| \quad (3..5)$$

therefore the attractive force is:

$$F_a(\mathbf{x}) = k_a \|(\mathbf{x}^* - \mathbf{x})\| \quad (3..6)$$

where $d_a = \|(\mathbf{x}^* - \mathbf{x})\| = \sqrt{(x^* - x)^2 + (y^* - y)^2}$ is the Euclidean distance between the goal postion $\mathbf{x}^* = (x^*, y^*)^T$ and the nanorobot position $\mathbf{x} = (x, y)^T$.

3.2.2. Repulsive potential field

In contrast to the attractive PF, the repulsive PF is more potent when the nanorobot is situated in close proximity to the obstacle. Any impediment that is located at a greater distance will not likely contribute to the total PF. Consequently, if the nanorobot's distance from the n -th obstacle, $d_o^{(n)}$, exceeds a threshold value τ , the respected PF is not considered, resulting in $U_r^{(n)}(\mathbf{x}) = 0$. Alternately, the repulsive PF is proportional to the inverse of the distance between the obstacle and the automaton [24], [25]. Let determine the repulsive function as:

$$U_r^{(n)}(\mathbf{x}) = \begin{cases} \frac{1}{2}k_r \left(\frac{1}{d_o^{(n)}}\right)^2 & \text{if } d_o^{(n)} \leq \tau \\ 0 & \text{if } d_o^{(n)} > \tau \end{cases} \quad (3..7)$$

where $d_o^{(n)} = \|(\mathbf{x}_o^{(n)} - \mathbf{x})\| = \sqrt{(x_o^{(n)} - x)^2 + (y_o^{(n)} - y)^2}$ is the Euclidean distance between the nanorobot position $\mathbf{x} = (x, y)^T$ and the n -th obstacle position $\mathbf{x}_o^{(n)} = (x_o^{(n)}, y_o^{(n)})^T$. Assuming that each obstacle possesses the same repulsive PF characteristic, the repulsive PF constant is represented by k_r . The repulsive force or negative gradient, is calculated as:

$$-\nabla_{\mathbf{x}} U_r^{(n)}(\mathbf{x}) = -\frac{\partial U_r^{(n)}(\mathbf{x})}{\partial \mathbf{x}} = F_r^{(n)}(\mathbf{x}) = \begin{cases} \frac{k_r}{(d_o^{(n)})^3} & \text{if } d_o^{(n)} \leq \tau \\ 0 & \text{if } d_o^{(n)} > \tau \end{cases} \quad (3..8)$$

3.3. Nanorobot control for obstacle avoidance

Nanorobots can autonomously navigate intricate microstructures by combining vision-based control systems, magnetic field manipulation, adaptive motion control, reinforcement learning, and advanced path-planning algorithms. Nanorobots can identify and evade obstructions in real time owing to the collective application of these technologies, which guarantees precise and efficient mobility in dynamically changing environments.

Prior to further developing the control rule for robot motion to evade obstacles, it is essential to decompose all forces, both attracting and repulsive, into their projections along the x -axis and y -axis [24], [25]. Consequently, the breakdown of the attractive force is calculated as:

$$F_{a,x} = -\nabla_x U_a(\mathbf{x}) \quad (3.9)$$

$$= k_a(x^* - x) \quad (3.10)$$

note that $d_a = \sqrt{(x^* - x)^2 + (y^* - y)^2}$ and $F_{a,x}$ is the attractive force in the x -axis direction. Moreover, the attractive force in y -axis direction is denoted as:

$$F_{a,y} = k_a(y^* - y) \quad (3.11)$$

the projections of the repulsive force along the x -axis and y -axis are as follows (note: the derivation considers just the case when $d_o^{(n)} \leq \tau$):

$$F_{r,x}^{(n)} = -\nabla_x U_r^{(n)}(\mathbf{x}) \quad (3.12)$$

$$= k_r \frac{(x_o^{(n)} - x)}{(d_o^{(n)})^4} \quad (3.13)$$

where $F_{r,x}^{(n)}$ represents the repulsive force exerted by the n -th obstacle along the x -axis. The identical deduction is applicable to ascertain the repulsive force in the y -axis direction, where:

$$F_{r,y}^{(n)} = k_r \frac{(y_o^{(n)} - y)}{(d_o^{(n)})^4} \quad (3.14)$$

therefore, the total force $F(\mathbf{x}) = (F_x, F_y)^T$ can be calculated as:

$$F_x = F_{a,x}(\mathbf{x}) + \sum_{n=1}^N F_{r,x}^{(n)}(\mathbf{x}) \quad (3.15)$$

$$F_y = F_{a,y}(\mathbf{x}) + \sum_{n=1}^N F_{r,y}^{(n)}(\mathbf{x}) \quad (3.16)$$

finally, the force direction can be computed as:

$$\theta = \arctan \frac{F_y}{F_x} \quad (3.17)$$

therefore, the velocity control signal $\mathbf{v} = (v_x, v_y)^T$ is determined by the total PF force in the simplest nanorobot control algorithm.

$$v_x = F_x \quad (3.18)$$

$$v_y = F_y \quad (3.19)$$

Then the nanorobot position can be updated by:

$$x(k) = x(k-1) + v_x \Delta t \quad (3.20)$$

$$y(k) = y(k-1) + v_y \Delta t \quad (3.21)$$

where Δt is the sampling time, $x(k)$ and $y(k)$ are the nanorobot x and y coordinates at k -th time instant.

The key design parameters in this work include the attractive constant k_a , the repulsive constant k_r , and the repulsive threshold distance τ . These parameters were chosen through empirical tuning and theoretical stability considerations to ensure smooth convergence without oscillation. In practice, a high k_a increases convergence speed but may lead to overshooting near the target, while a high k_r improves obstacle avoidance but can result in unnecessary detours. The threshold τ was determined based on the nanorobot size and the expected biological barrier distance, typically 2–5 times the nanorobot diameter. Optimal parameters were obtained by iterative tuning across four simulation states until the nanorobot reached the target with minimal path error.

4. RESULTS AND DISCUSSION

Algorithm testing was conducted using a series of simulations that modelled four distinct conditions. In the initial simulation, the nanorobot navigated an environment with static obstacles and targets. The second simulation incorporated static obstacles with dynamic targets. In the third, the obstacles were dynamic while the target remained static. The fourth simulation integrated both dynamic obstacles and dynamic targets. In all instances, the F_a and F_r values were maintained constant. The coordinates of the obstacles and targets were modified to represent static or dynamic conditions. The simulation results are presented below. Figure 1 illustrate general flowchart to explain the simulation process performed on the nanorobot motion study.

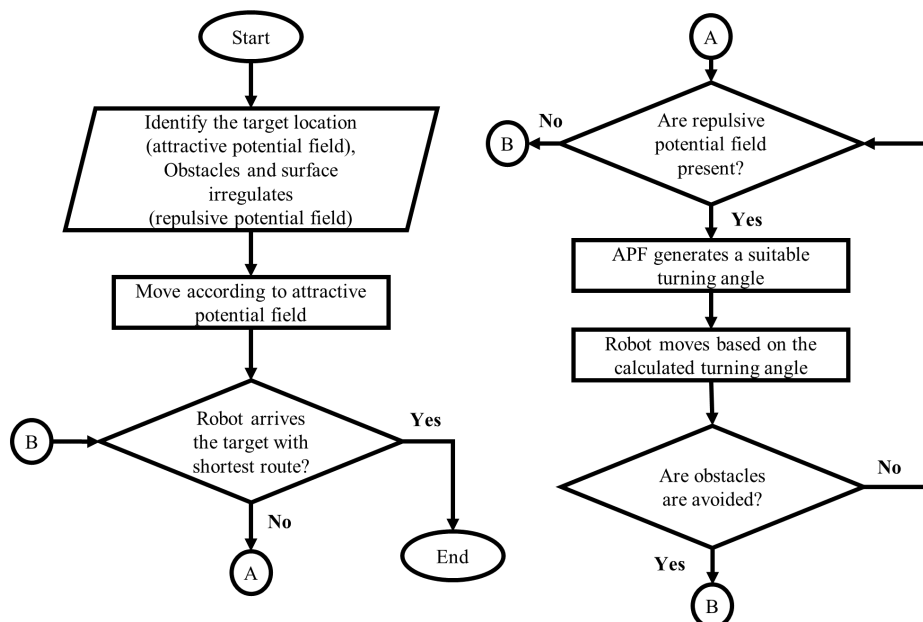


Figure 1. General flowchart to explain the simulation process performed on the nanorobot motion study

4.1. Nanorobot motion with a static target and static obstacle

The simulation was conducted by performing two trials, with a fixed target coordinate point $x = 10$, $y = 5$, and a fixed starting point with coordinate $x = 0$, $y = 0$. Additionally, four obstacles were positioned in two different location schemes. The positions of the obstacles can be seen in Table 1.

Figure 2 shows test results of nanorobot movement with first condition. Based on the simulation results shown in Figure 2(a) and Figure 2(b), it can be observed that the nanorobot can maneuver to avoid obstacles to reach the target coordinate point. It is evident that when the nanorobot approaches an obstacle and enters the repulsive region of the obstacle, the nanorobot can move towards a lower repulsive area (the magnitude of the repulsive force is indicated by the darkness of the blue color around the obstacle area).

4.2. Nanorobot motion with a dynamic target and static obstacle

The simulation was conducted by performing two tests, with a fixed starting point with coordinate $x = 0$, $y = 0$. Additionally, two different dynamic target coordinate points, which is: i) moving target which moving from $x = 8.0$, $y = 3.0$ into $x = 6.0$, $y = 8.0$ and ii) moving target which moving from $x = 10.0$, $y = 5.0$ into $x = 10.0$, $y = 0.0$. Moreover, four obstacles were positioned in two different locations for each scheme. The positions of the obstacles can be seen in Table 1.

Table 1. Obstacle configuration for each scheme under condition I and II

Obstacle	Scheme 1		Scheme 2	
	x	y	x	y
1	2.0	2.0	2.0	2.0
2	3.0	1.0	3.0	1.0
3	7.0	2.5	5.0	4.0
4	7.5	1.5	6.0	4.5

Figure 2 shows test results of nanorobot movement with second condition. Based on the simulation results shown in Figure 2(c) and Figure 2(d), it can be observed that the nanorobot can maneuver to avoid obstacles to reach the target coordinate, which is also in motion into the final position. In the previous results, the nanorobot also avoids obstacles based on the repulsive force and the attractive force from the target, and the attractive force from the target varies in value because the target destinations of the nanorobot are also in motion. It enables the nanorobot to maneuver with different variations, adapting to the movements of the target being pursued. The maneuver variations generated also depend on the closest trajectory of the nanorobot to the moving target.

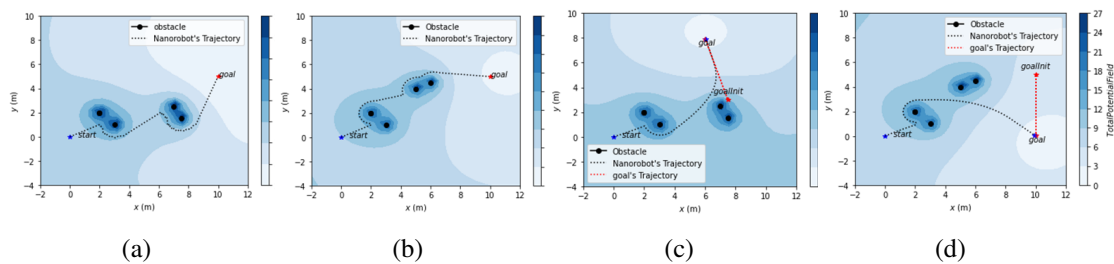


Figure 2. Nanorobot movement test results under different simulation conditions (a) and (b) Condition I (Static target and static obstacles) for Scheme 1 and Scheme 2. (c) and (d) Condition II (Dynamic target and static obstacles) for Scheme 1 and Scheme 2

4.3. Nanorobot motion with a static target and dynamic obstacle

The simulation was conducted by performing two trials, with a fixed target coordinate point $x = 8$, $y = 6$, fixed starting point with coordinate $x = 0$, $y = 0$, and two obstacles were positioned in two different locations that moved into a specific location for each scheme. The positions of the obstacles can be seen in Table 2.

Table 2. Obstacle configuration for each scheme under condition III

Obstacle	Scheme 1				Scheme 2			
	Initial pose		Final pose		Initial pose		Final pose	
	x	y	x	y	x	y	x	y
1	2.0	2.0	3.0	-1.0	2.0	1.0	6.5	4.0
2	8.0	5.0	5.5	4.5	7.0	5.0	6.0	2.0

Figure 3 shows test results of nanorobot movement with second condition. Based on the simulation results shown in Figure 3(a) and Figure 3(b), it can be observed that the nanorobot can maneuver to avoid obstacles to reach the target coordinate even if the obstacles are also in motion. The nanorobot can respond to moving obstacles, as demonstrated when the nanorobot encounters a suddenly appearing obstacle.

The nanorobot can maneuver to alter its trajectory to avoid collision with the obstacle. In the figure, the trajectory of the obstacle is shown in red, while the nanorobot's trajectory is shown in black. At specific points in the figure, marked as collision points, it represents the locations where the nanorobot encounters the obstacle. However, before a collision occurs, the nanorobot maneuvers to avoid the obstacle while moving towards the predetermined target coordinate point. As seen in both results figures, the nanorobot can instantly react to the obstacles motion by maneuvering.

4.4. Nanorobot motion with a dynamic target and dynamic obstacle

The simulation was conducted by performing two trials, with a fixed starting point with coordinate $x = 0, y = 0$. Additionally, two different dynamic target coordinate points, which is: i) moving target which moving from $x = 8.0, y = 0.0$ into $x = 8.0, y = 7.0$ and ii) moving target which moving from $x = 8.5, y = 4.0$ into $x = 2.0, y = 8.0$. Furthermore, two up to three obstacles were positioned in different locations that moved into a specific location for each scheme. The positions of the obstacles can be seen in Table 3.

Figure 3 shows test results of nanorobot movement with second condition. Based on the simulation results shown in Figure 3(c) and Figure 3(d), it can be observed that the nanorobot can maneuver to avoid obstacles to reach the target coordinate, even if the obstacles are also in motion. The results indicate that the nanorobot can move towards a moving target by adjusting its trajectory to chase the movement of that target point. During the pursuit of the target point's movement, the nanorobot encounters moving obstacles that can potentially lead to collisions. However, from the executed simulation, the nanorobot can maneuver to avoid suddenly appearing obstacles while maintaining its movement towards the target destination. Therefore, through these maneuvers, it is evident that the nanorobot can move agilely to avoid moving obstacles while still preserving its direction towards the moving target point.

Table 3. Obstacle configuration for each scheme under condition IV

Obstacle	Scheme 1				Scheme 2			
	Initial pose		Final pose		Initial pose		Final pose	
	x	y	x	y	x	y	x	y
1	2.0	1.0	7.0	0.75	2.0	2.0	4.5	2.0
2	7.5	5.0	6.0	2.0	8.0	0.0	5.0	2.5
3	-	-	-	-	4.0	4.0	5.5	5.5

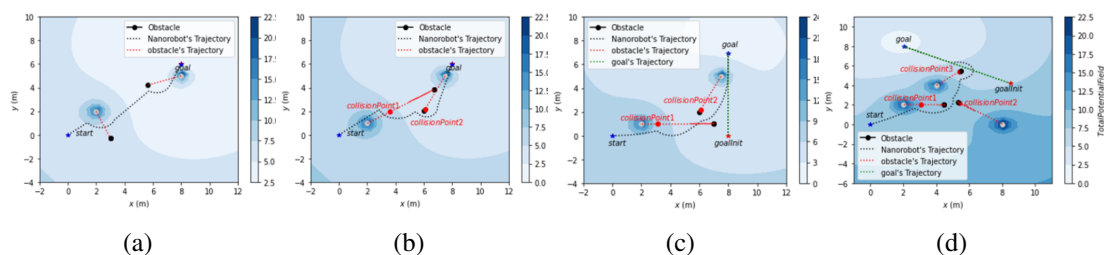


Figure 3. Nanorobot movement test results under different simulation conditions (a) and (b) Condition III (Static target and Dynamic obstacles) for Scheme 1 and Scheme 2. (c) and (d) Condition IV (Dynamic target and Dynamic obstacles) for Scheme 1 and Scheme 2

5. CONCLUSION

This study has illustrated the efficacy of PF-based methodologies in improving the autonomous navigation of nanorobots for medication delivery purposes. Utilizing appealing and repulsive virtual forces, nanorobots may adeptly navigate intricate biological settings while reducing collision hazards. The simulation outcomes validate that PF techniques facilitate accurate path planning, even in dynamic environments with mobile barriers and targets. Conventional PF methods encounter obstacles, including local minima and restricted adaptation to rapidly changing physiological conditions. Hybrid PF approaches that integrate global optimization, reinforcement learning, and velocity-dependent modifications present viable options to address these limitations. Future research must prioritize experimental validation in authentic biological settings and

the integration of multi-modal control mechanisms to improve navigation efficiency. This study's findings enhance the development of intelligent nanorobotic systems for targeted drug delivery, facilitating more efficient and least intrusive therapeutic interventions.

FUNDING INFORMATION

Authors state no funding involved.

AUTHOR CONTRIBUTIONS STATEMENT

This journal uses the Contributor Roles Taxonomy (CRediT) to recognize individual author contributions, reduce authorship disputes, and facilitate collaboration.

Name of Author	C	M	So	Va	Fo	I	R	D	O	E	Vi	Su	P	Fu
Leonardo Kamajaya	✓	✓		✓	✓	✓			✓	✓	✓			
Indrazno Siradjuddin		✓	✓	✓		✓				✓		✓		
Gillang Al Azhar	✓	✓	✓	✓		✓		✓	✓	✓	✓	✓		
Fitri	✓							✓		✓			✓	✓
Agwin Fahmi Fahanani	✓			✓						✓		✓		

C : Conceptualization

I : Investigation

Vi : Visualization

M : Methodology

R : Resources

Su : Supervision

So : Software

D : Data Curation

P : Project administration

Va : Validation

O : Writing - Original Draft

Fu : Funding acquisition

Fo : Formal analysis

E : Writing - Review & Editing

CONFLICT OF INTEREST STATEMENT

Authors state no conflict of interest.

DATA AVAILABILITY

The authors confirm that all data supporting the findings of this study are available within the article.




REFERENCES

- [1] K. Xu and J. Zhou, "Drug delivery for micro-/nanorobots: progress and challenges," *Current Nanoscience*, vol. 18, no. 6, pp. 690–699, 2022, doi: 10.2174/1573413718666220127123038.
- [2] T. K. Ramchandani, "A brief review on nanorobotics," *International Journal for Research in Applied Science and Engineering Technology*, vol. 11, no. 12, pp. 1301–1306, 2023, doi: 10.22214/ijraset.2023.57591.
- [3] H. Zhou, C. C. Mayorga-Martinez, S. Pané, L. Zhang, and M. Pumera, "Magnetically driven micro and nanorobots," *Chemical Reviews*, vol. 121, no. 8, pp. 4999–5041, 2021, doi: 10.1021/acs.chemrev.0c01234.
- [4] Y. Hanli, L. Qiliang, and Z. Weizhen, "Robot obstacle avoidance based on improved artificial potential field method," in *10th International Conference on Control, Automation and Information Sciences, ICCAIS 2021 - Proceedings*, 2021, pp. 769–775, doi: 10.1109/ICCAIS52680.2021.9624644.
- [5] O. Montiel, U. Orozco-Rosas, and R. Sepúlveda, "Path planning for mobile robots using bacterial potential field for avoiding static and dynamic obstacles," *Expert Systems with Applications*, vol. 42, no. 12, pp. 5177–5191, 2015, doi: 10.1016/j.eswa.2015.02.033.
- [6] S. Amoh, D. Ito, and T. Ueta, "A method to suppress local minima for symmetrical DOPO networks," *Nonlinear Theory and Its Applications, IEICE*, vol. 11, no. 4, pp. 580–589, 2020, doi: 10.1587/nolta.11.580.
- [7] N. He, Y. Su, J. Guo, X. Fan, Z. Liu, and B. Wang, "Dynamic path planning of mobile robot based on artificial potential field," in *Proceedings - 2020 International Conference on Intelligent Computing and Human-Computer Interaction, ICHCI 2020*, 2020, pp. 259–264, doi: 10.1109/ICHCI51889.2020.00063.
- [8] H. Li, "Robotic path planning strategy based on improved artificial potential field," in *Proceedings - 2020 International Conference on Artificial Intelligence and Computer Engineering, ICAICE 2020*, 2020, pp. 67–71, doi: 10.1109/ICAICE51518.2020.00019.
- [9] Y. Li, B. Tian, Y. Yang, and C. Li, "Path planning of robot based on artificial potential field method," in *IEEE 6th Information Technology and Mechatronics Engineering Conference, ITOEC 2022*, 2022, vol. 6, pp. 91–94, doi: 10.1109/ITOEC53115.2022.9734712.
- [10] R. Szczepanski, A. Bereit, and T. Tarczewski, "Efficient local path planning algorithm using artificial potential field supported by augmented reality," *Energies*, vol. 14, no. 20, p. 6642, 2021, doi: 10.3390/en14206642.
- [11] D. Zhang, G. Zhu, and Q. Zhang, "Multi-robot motion planning: a learning-based artificial potential field solution," in *Proceedings of the 2nd Conference on Fully Actuated System Theory and Applications, CFASTA 2023*, 2023, pp. 233–238, doi: 10.1109/CFASTA57821.2023.10243195.




- [12] R. Wang, J. Guo, S. Guo, Q. Fu, and J. Xu, "Cooperative hunting of spherical multi-robots based on improved artificial potential field method," in *2022 IEEE International Conference on Mechatronics and Automation, ICMA 2022*, 2022, pp. 575–580, doi: 10.1109/ICMA54519.2022.9856156.
- [13] S. Fusco *et al.*, "Shape-switching microrobots for medical applications: the influence of shape in drug delivery and locomotion," *ACS Applied Materials and Interfaces*, vol. 7, no. 12, pp. 6803–6811, 2015, doi: 10.1021/acsami.5b00181.
- [14] A. C. Hortelão, T. Patiño, A. Perez-Jiménez, À. Blanco, and S. Sánchez, "Enzyme-powered nanobots enhance anticancer drug delivery," *Advanced Functional Materials*, vol. 28, no. 25, p. 1705086, 2018, doi: 10.1002/adfm.201705086.
- [15] L. Huang, F. Chen, Y. Lai, Z. Xu, and H. Yu, "Engineering nanorobots for tumor-targeting drug delivery: from dynamic control to stimuli-responsive strategy," *ChemBioChem*, vol. 22, no. 24, pp. 3369–3380, 2021, doi: 10.1002/cbic.202100347.
- [16] W. Y. Jeong, M. Kwon, H. E. Choi, and K. S. Kim, "Recent advances in transdermal drug delivery systems: a review," *Biomaterials Research*, vol. 25, no. 1, p. 24, 2021, doi: 10.1186/s40824-021-00226-6.
- [17] A. M. Vargason, A. C. Anselmo, and S. Mitragotri, "The evolution of commercial drug delivery technologies," *Nature Biomedical Engineering*, vol. 5, no. 9, pp. 951–967, 2021, doi: 10.1038/s41551-021-00698-w.
- [18] B. Zhang, L. Zhu, H. Pan, and L. Cai, "Biocompatible smart micro/nanorobots for active gastrointestinal tract drug delivery," *Expert Opinion on Drug Delivery*, vol. 20, no. 10, pp. 1427–1441, 2023, doi: 10.1080/17425247.2023.2270915.
- [19] W. Siti, H. L. Too, T. Anderson, X. R. Liu, I. Y. Loh, and Z. Wang, "Autonomous DNA molecular motor tailor-designed to navigate DNA origami surface for fast complex motion and advanced nanorobotics," *Science Advances*, vol. 9, no. 38, p. eadi8444, 2023, doi: 10.1126/SCIADV.ADI8444.
- [20] F. Soto, J. Wang, R. Ahmed, and U. Demirci, "Medical micro/nanorobots in precision medicine," *Advanced Science*, vol. 7, no. 21, p. 2002203, 2020, doi: 10.1002/adv.202002203.
- [21] Z. Wu, Y. Chen, D. Mukasa, O. S. Pak, and W. Gao, "Medical micro/nanorobots in complex media," *Chemical Society Reviews*, vol. 49, no. 22, pp. 8088–8112, 2020, doi: 10.1039/d0cs00309c.
- [22] L. Mertz, "Enhancing therapeutic delivery using micro- and nanorobots," *IEEE Pulse*, vol. 14, no. 2, pp. 18–22, 2023, doi: 10.1109/MPULS.2023.3269754.
- [23] Z. Sun and Y. Hou, "Micro/nanorobots as active delivery systems for biomedicine: from self-propulsion to controllable navigation," *Advanced Therapeutics*, vol. 5, no. 7, p. 2100228, 2022, doi: 10.1002/adtp.202100228.
- [24] I. Siradjuddin *et al.*, "Mobile robot with independent steering and driving and obstacle avoidance using an artificial potential field," in *AIP Conference Proceedings*, 2024, vol. 2927, no. 1, p. 40012, doi: 10.1063/5.0205228.
- [25] K. Nurhalim, I. Siradjuddin, and R. I. Putri, "Implementasi algoritma potensial field obstacle avoidance pada robot beroda 4 omni wheels simetris," *Journal of Applied Smart Electrical Network and Systems*, vol. 3, no. 01, pp. 16–24, Jun. 2022, doi: 10.52158/jasens.v3i01.417.

BIOGRAPHIES OF AUTHORS






Leonardo Kamajaya    is a lecturer in electronic engineering study program at State Polytechnic of Malang. He received a bachelor's degree in electronic engineering at Politeknik Elektronika Negeri Surabaya and a master's degree in electrical engineering at Chang Gung University. His research interests include a biosensor, electronics systems, electronics projects based on the IoT and renewable energy. He can be contacted at email: leonardo42@polinema.ac.id.






Indrazno Siradjuddin    received the B.E. and master degrees in electrical engineering from Brawijaya University, Indonesia, in 2000 and from Institut Teknologi Sepuluh Nopember, Indonesia, in 2004, and the Ph.D. degree in computing and engineering from the University of Ulster, U.K, in 2014. He is currently an associate professor in the Department of Electrical Engineering, State Polytechnic of Malang, Indonesia. He has more than 160 papers to his credit published in refereed journals and conference proceedings. His research interests include intelligent control, robotics, neural networks, and cognitive modelling. He can be contacted by email: indrazno@polinema.ac.id.






Gillang Al Azhar    is a lecturer in the Department of Electrical and Electronic Engineering at State Polytechnic of Malang, Indonesia. He holds a master of engineering degree and specializes in mobile robotics. His expertise includes robot operating system (ROS), C programming, Python, Arduino, and AVR microcontrollers. His research interests focus on improving the accuracy and performance of mobile robotic systems. He has worked on implementing g-h filters to enhance compass sensor accuracy for differential drive robot trajectory tracking and has contributed to the development of data distribution control systems using ROS for mobile robots. He can be contacted at email: gillang_al.azhar@polinema.ac.id.



Fitri    is a lecturer in electronic engineering study program at State Polytechnic of Malang. She received bachelor's and master's degrees at Brawijaya University. Her research interests include a sensor, renewable energy and embedded system. She can be contacted by email: fitri@polinema.ac.id.



Agwin Fahmi Fahanani    is a biomedical engineering researcher and lecturer in medical bachelor in Faculty of Medicine, Universitas Brawijaya, Malang, Indonesia. He received a bachelor's degree in electrical engineering at Universitas Brawijaya and a master's degree in electrical engineering (biomedical engineering concentration) at Institut Teknologi Bandung. His research interests include medical image processing, biosensor, and medical devices. He can be contacted at email: agwinfahmi@ub.ac.id.